*Scientific paper*

# Modeling and Analysis of Shear-critical ECC Members with Anisotropic Stress and Strain Fields

Benny Suryanto[1], Kohei Nagai[2] and Koichi Maekawa[3]

## Abstract

This paper describes an attempt to predict the response of shear-critical ECC members that exhibit strong anisotropic stress and strain fields. The ECC members investigated include pre-cracked ECC plates under stress field rotation, orthogonally-reinforced ECC (R/ECC) panel under pure shear, and shear-critical R/ECC beams under reversed cyclic loading. To achieve a simple yet accurate prediction, the mechanics of the ECC are represented by smeared models using a fixed crack approach. The applicability of these models is demonstrated through a simulation of ECC plates and R/ECC panel responses. This demonstrates the importance of an appropriate shear transfer model in representing essential behaviors of ECC in an anisotropic field. Predictions of these models were then compared against experimental results of shear-critical R/ECC beams with a M/Vd ratio of 1.0 and 0.5. For beams with a M/Vd ratio of 1.0, a good agreement is observed in terms of hysteretic response, crack pattern, and failure mechanisms. For beams with a 0.5 M/Vd ratio, the analysis somewhat underestimates the beam capacity, although it does predict a correct failure mechanism. Overall, this paper demonstrates that practical application of nonlinear finite-element analysis to ECC structural members is possible.

## 1. Introduction

Engineered Cementitious Composite is a fiber-reinforced cement-based material that when pulled exhibits multiple cracking, ductile, and a strain hardening response. In the past two decades, a number of experiments have been undertaken to apply ECC to shear-critical structural members (Li *et al* 1994; Kanda 1998; Fukuyama *et al* 2000; Shimizu *et al* 2004; Nagai *et al* 2004; Kanakubo *et al* 2007 among other). These experiments have demonstrated the following advantages in using ECC: namely, improvement of structural and deformational capacities, ductile failure, and high damage tolerance. However, there is still limited quantitative studies available relating to the response of shear-critical R/ECC members.

Previous quantitative studies in this area were primarily conducted by Kabele (1995, 1999, 2001, 2003, 2004, 2006, and 2007). In his pioneering work in 1995, an analytical procedure combining the plasticity-based theory and the discrete crack approach was proposed. The proposed analytical procedure has been observed to be advantageous for studying the fracture behavior of ECC. Nevertheless, it was less accurate in situations where crack slip is dominant. Improvements were made

in 1999 and 2001 in which a smeared fixed crack approach was used. This approach allows for the separate modeling of tensile and shear stresses at crack locations. Cracked ECC in the crack-slip direction were represented as two ECC bodies connected by a number of stocky elastic beams, while cracks in the crack-opening direction were modeled according to uniaxial tensile test data. Kabele demonstrates that shear stiffness of the ECC had to be considerably reduced to replicate a load-deflection response of shear-critical reinforced ECC (R/ECC) beams under cyclic loading. In 2003, 2004, 2006 and 2007, a multi-scale modeling concept was introduced to the analytical procedure. Significant refinement was made to the tension model to account for the contributions of fiber bridging, while the shear model was kept unchanged. The procedure was then used to simulate the same beams under monotonic loading. It was found that the opening and the sliding of the diagonal cracks at the web of the beam are substantial, and hence responsible for the failure of the beam. This latest development, while significantly insightful, is still limited to a monotonic load and requires information of fiber-matrix interface properties that are typically difficult to obtain.

As an alternative approach, Suwada and Fukuyama (2006b) employed the smeared rotating crack model and analyzed the shear-critical elements governed by diagonal tensile and compression failure. Analysis results showed a strong correlation once the compression-softening effects due to transverse cracking were considered. This approach was, however, limited to situations where monotonic loading is applied. It should be noted that although a rotating crack approach offers advantages under monotonic loading conditions, it often

[1]JSPS Postdoctoral Research Fellow, Department of Civil Engineering, University of Tokyo, Japan.
*E-mail*: benny@concrete.t.u-tokyo.ac.jp
[2]Lecturer, Department of Civil Engineering, University of Tokyo, Japan.
[3]Professor, Department of Civil Engineering, University of Tokyo, Japan.

has poor accuracy when applied to general loading conditions. Another alternative approach was proposed by Boshoff and Van Zijl (2007), who developed a computational scheme that is based on an isotropic damage concept to analyze the results of Iosipescu shear tests. It was reported that a further improvement is still necessary to take into account the beneficial effects of biaxial loading. This proposed approach is also limited to a monotonic load.

Presented herein is an alternative procedure of the smeared, fixed crack approach which provides an insight on the nonlinear mechanics of ECC under arbitrary in-plane stress conditions as well as provides accurate simulations of ECC responses under reversed cyclic loading. Path-dependent compression, tension, and shear transfer models of ECC in this context are proposed. All of these were identified from previously reported experiments. The identification of the shear transfer model was somewhat indirect because of a lack of understanding regarding the behavior associated with interface shear transfer in ECC. This was finally accomplished by rationalizing the behavior of pre-cracked ECC plates subjected to principal stress rotation (Suryanto 2009) and R/ECC panel that is subjected to pure shear (Xoxa 2003). During the identification, it was found that the tensile property of the ECC in a structural member differs to some extent from that obtained from a uniaxial tensile test. This finding is presented together in a discussion of the importance of a proper shear transfer model.

To demonstrate the validity of the proposed models, this paper presents a simulation of four shear-critical R/ECC beams, both with and without web reinforcement, subjected to reverse cyclic loading. In particular, the ability of the models to account for previous loading history, to capture the preexisting damage, and to take the effects into account for the remaining responses is presented. This simulation is expected to provide some insight into the behavior of ECC while being subjected to complex loading history. The predicted load capacity was also compared to the predicted values based on the AIJ shear design equation (after somewhat modified to include the contribution of ECC in tension), and to those reported previously by Kabele (2001, 2006).

## 2. Material modeling of R/ECC using the smeared concept

The ECC models proposed in this paper were modified from the two-dimensional constitutive models of reinforced concrete in which full documentation of the original models is available in Maekawa *et al* (2003). In general, the ECC models proposed retain all fundamental features of the original models, including the path-dependent formulations, and the assumption of average stress and average strain rooted in each model. To deal with ECC, modifications were made to the formulations describing the monotonic response of the models. The formulations describing the internal unloading-reloading loop were found to be sufficiently accurate and therefore were directly adopted.

### 2.1 Compression model
The compression model adopted is essentially the same as the concrete model referred to as the elasto-plastic fracture model. A slight modification was made to the strain corresponding to the compression strength $\varepsilon_c$, which represents the peak of the stress-strain curve. This strain is modified from a value of about 0.2% to a value in the range of 0.4% to 0.6%, which can be approximated from a cylinder test. As illustrated in **Fig. 1(a)**, this modification results in a softer compression response, marked by a softer ascending branch of the monotonic curve and a lower stiffness of the internal unloading-reloading loops.

An important aspect of the proposed model is the compressive strength reduction factor $\omega_c$. This factor is hypothesized based on the effects of transverse cracking and comparable to that considered for cracked concrete. Although a comprehensive study has *not* been carried out for ECC, the effects from the available test data reported by Suwada and Fukuyama (2006b) were taken into account. **Figure 1(b)** shows the proposed softening model which is derived by:

$$\omega_c = 1 - \left( \frac{2\varepsilon_{t,\max}}{1 + 5\varepsilon_{t,\max}} \right) \tag{1}$$

where $\varepsilon_{t,max}$ is the maximum tensile strain normal to cracks and defined in %.

**Figure 1(c)** shows a comparison between the cylinder responses tested by Xoxa (2003) and Suryanto (2009) and the predicted compressive stress-strain obtained from the original and modified models of concrete and ECC, respectively. For two different compressive strength levels investigated, the agreement is good.

### 2.2 Tension model
It has been proposed by Kanda (1998) that the tensile response of PVA-ECC can be reasonably represented by a bi-linear stress-strain relationship up to the peak tensile stress. A similar representation is adopted herein. The post-peak response is tentatively assumed to decrease linearly from the maximum tensile stress $f_{t,max}$ to zero at $\varepsilon_{t,o}$. The tension-stiffening effect at the post-peak region may be significant and hence should be further addressed.

$$f_t = \omega_t \left( E_i \varepsilon \right) \quad \text{for} \quad 0 \le \varepsilon \le \varepsilon_{t,cr} \tag{2}$$

$$f_t = \omega_t \left[ f_{t,cr} + E_{sh} \left( \varepsilon - \varepsilon_{t,cr} \right) \right] \quad \text{for} \quad \varepsilon_{t,cr} < \varepsilon \le \varepsilon_{t,u} \tag{3}$$

$$f_t = \omega_t \left[ f_{t,u} - E_{sf} \times \left( \varepsilon - \varepsilon_{t,u} \right) \right] \quad \text{for} \quad \varepsilon_{t,u} < \varepsilon \le \varepsilon_{t,o} \tag{4}$$
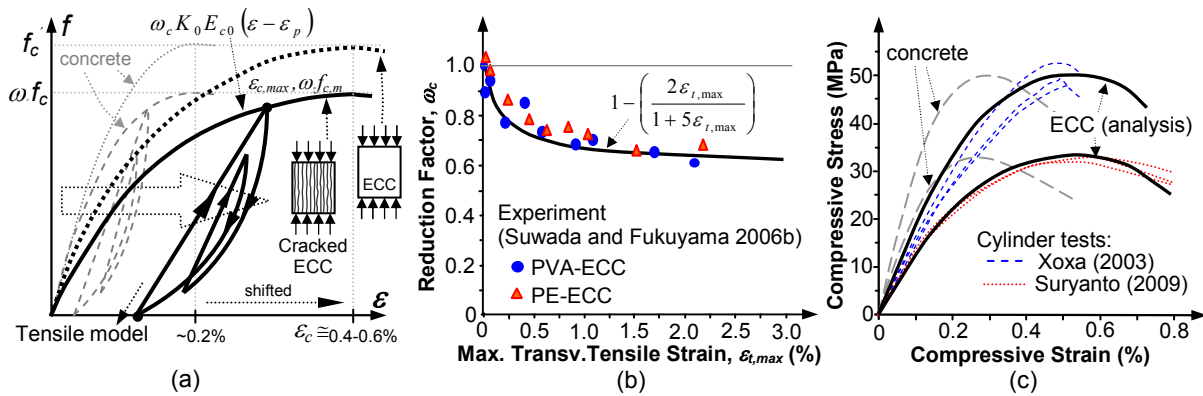
Fig. 1 Compression model: (a) Cracked concrete model versus the modified model; (b) Strength reduction factor due to transverse cracking; (c) Model verification.
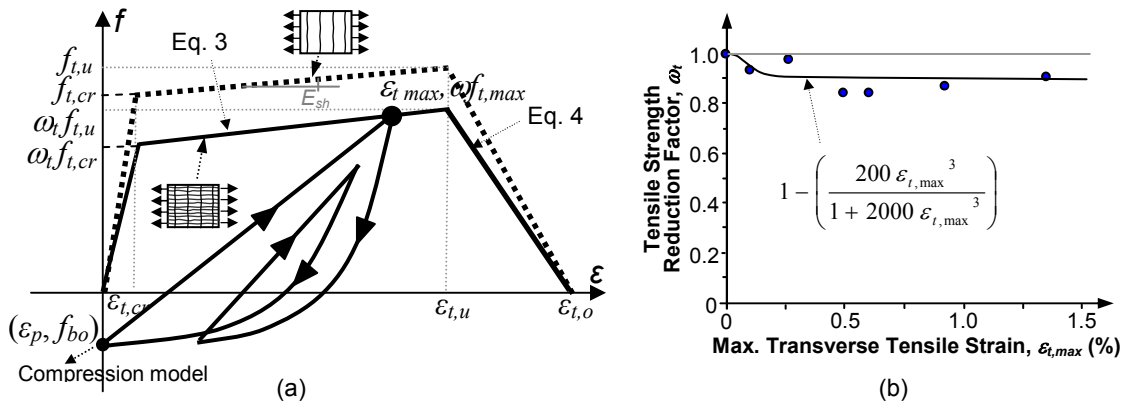


Fig. 2 Tension model: (a) Basic model; (b) Tensile strength reduction factor due to transverse cracking.

$$f_t = 0 \qquad \text{for} \quad \varepsilon > \varepsilon_{t,o} \tag{5}$$

In this model, it is considered that transverse cracking also weakens to the tensile strength and stiffness of PVA-ECC. These effects are approximated from experiments of PVA-ECC plates containing longitudinal pre-cracks on the bottom surface that were tested using a four-point bending scheme (Suryanto 2009). This result suggests that the weakening effects increase as the maximum transverse tensile strain increases: namely,

$$\omega_t = 1 - \left( \frac{200\varepsilon_{t,\max}{}^3}{1 + 2000\varepsilon_{t,\max}{}^3} \right) ; \; \varepsilon_{t,max} \text{ in } \% \tag{6}$$

To represent the unloading-reloading path of the tensile model, this study adopts the path used in the original formulations of concrete, which has a nonlinear unloading path and linear reloading path. Test data reported by Kesner *et al* (2003) and Suwada and Fukuyama (2006a) revealed that both unloading and reloading responses of ECC reinforced with PVA fibers are actually nonlinear. The reloading shape, prior to the attainment of compressive strength, is nearly linear, and

hence it is assumed to be linear.

## 2.3 Verification of the compression and tensile models

This subsection describes the applicability of the proposed models while representing the behavior of ECC under reversed cyclic loading. **Figure 3(a)** presents the analysis result of an element subjected to reverse cyclic loading, plotted against the response of Specimen PVA1 tested by Kesner *et al* (2003). The test specimen was a cylinder with a diameter of 50 mm and was tested alternately in compression and in tension at a strain rate of 0.1% per min. As shown, the correlation until one cycle following the attainment of the compressive strength is reasonably good, confirming the applicability of the models.

To further examine the applicability of the proposed models, consider the cyclic response of a-21-mm-thick ECC plate shown in **Fig. 3(b)**. The plate was tested in a four-point loading condition at a rate of 1 mm per min. The plate span was 340 mm and with a constant moment span of 170 mm. The cyclic reverse loading was done manually by flipping the plate upside down. Nu-

merical analysis was conducted to predict the response of this plate. Eight-node mindlin plates were used with mesh and material properties as shown. As can be seen, the predicted response provides a reasonable agreement with the observed response; both appear to develop a higher degree of stiffness degradation, a larger value of residual displacement, and an increased degree of pinching as the maximum displacement at each load cycle increases. These results reconfirm the applicability of the proposed models.

## 2.4 Shear transfer model

The shear model for PVA-ECC proposed herein attempts to account for the inherent contribution of shear friction and fiber bridging across cracks. **Figure 4(a)** shows the comparison of a typical shear response of cracked concrete (Li *et al* 1989) and a hypothetical shear response of cracked PVA-ECC. *In normal-strength concrete*, aggregate interlock enables two rough crack surfaces, when they slide over each other and when under a sufficient level of lateral confinement, to

develop a significant degree of shear resistance. *In PVA-ECC*, it is postulated that, owing to the absence of coarse aggregate, a significantly less shear resistance can develop across cracks and hence results in a pronounce crack slip. In this study, the shear transfer model adopted is that of Li *et al* (1989), which is applicable for *normal-strength* concrete. To comply with the reduced shear resistance and substantial slip of cracks in ECC, a reduction factor *A* was introduced to the model as given by:

$$v_{cr} = A.f_{st} \frac{\beta^2}{1+\beta^2} \tag{7}$$

where $v_{cr}$ is the shear stress transferred across a crack, $f_{st}$ is the maximum shear stress that can be transferred across a crack and is given by $f_{st} = 3.8 f_c^{'1/3}$ ($f_c^{'}$ in MPa), and $\beta$ is the ratio of crack slip ($\gamma_{cr}$) to crack opening ($\varepsilon_t$). It is expected that the *A* value should vary depending on the type and volume of the fibers used. It was found that
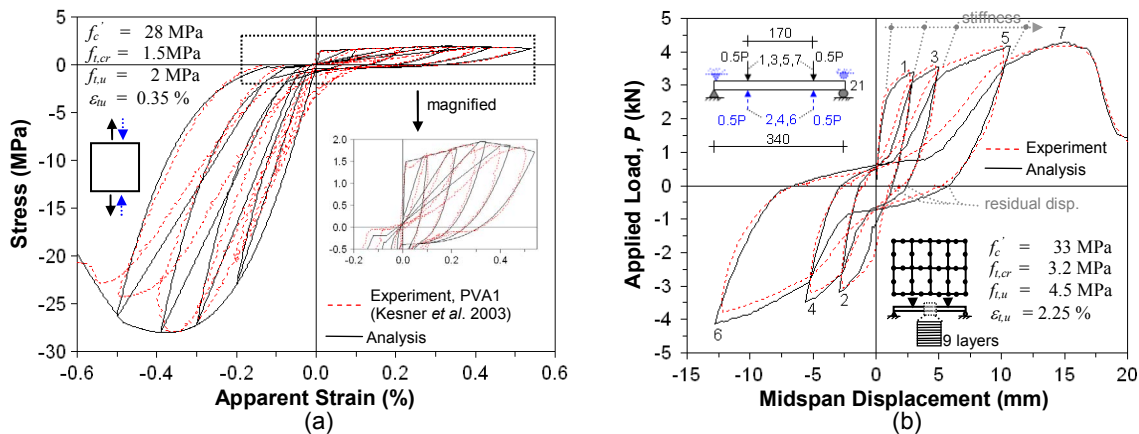


Fig. 3 Verification of compression-tension model on: (a) an element subjected to reverse cyclic loading plotted against the result of a 50-mm diameter ECC cylinder; and (b) a 250×340×21 mm plate subjected to reverse bending.
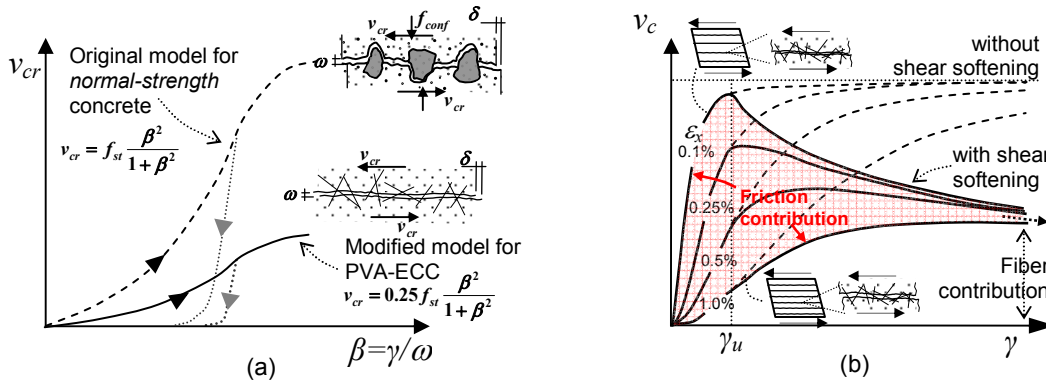


Fig. 4 Average shear stress-strain relationship of cracked PVA-ECC: (a) Basic model; (b) Enhanced model with shear softening.

a value of $A=0.25$ gives acceptable agreement for ECC containing approximately 2% by volume of PVA fibers (Suryanto 2009). The average shear stiffness of cracked PVA-ECC $G$ can be then obtained by following the procedure explained in details in Maekawa *et al* (2003).

It is also postulated that shear transfer across cracks in ECC is influenced by the crack opening as illustrated in **Fig. 4(b)**. While the crack opening is small, both crack-shear friction and fiber bridging contribute to the shear transfer resistance. As the crack opening increases, the frictional resistance diminishes, while the contribution of fiber bridging remains. The loss contribution of shear friction is treated as a shear softening phenomenon. To take this into account, the softening model previously used by An (1996) is adopted and is given by:

$$v_c = G\gamma \qquad \text{for } \gamma < \gamma_u \tag{8}$$

$$v_c = G\gamma \left(\frac{\gamma_u}{\gamma}\right)^c \qquad \text{for } \gamma \geq \gamma_u \tag{9}$$

where $v_c$ is the average shear stress, $G$ is the average shear stiffness of cracked PVA-ECC, $\gamma_u$ is the average shear strain from where the shear softening starts, and $c$ is the shear softening coefficient. It is expected that the values of $\gamma_u$ and $c$ relates to the degree of lateral confinement, which partly depends on the type and volume of the fibers. For ECC containing approximately 2% by volume of PVA fibers, it is proposed that the $\gamma_u$ is 1,000 and 4,000 micron for ECC and R/ECC, respectively. The $c$ parameter is suggested to be 0.4. If the volume of the fiber in the ECC is less than 2%, a greater $c$ value should be used.

## 2.5 Steel model

The monotonic stress-strain relation for reinforcing bar embedded in ECC is assumed to be linear elastic until yielding and then perfectly plastic, similar to the typical response of bare reinforcement. This assumption is made by the observation of Fischer and Li's test results (2002), who demonstrated a compatible deformation between reinforcement and the surrounding ECC. The hysteretic response of the bar is modeled after Kato (1979).

## 2.6 Verification of the material models

To check the suitability of the material models proposed, two verification problems were carried out. The first verification problem was on a test series of pre-cracked ECC plates subjected to principal stress rotation, while the second one was on R/ECC panel subjected to pure shear loading; with both underwent significant anisotropic stress and strain conditions during loading. The former addresses the importance of proper damage identification and suitable shear transfer representation in ECC, while the later addresses the significance of appropriate shear transfer and tensile property of ECC in R/ECC member. For the purpose of verification, the
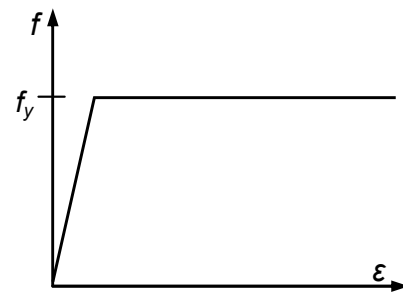


Fig. 5 Assumed average stress-strain relationship of reinforcement embedded in cracked ECC.

proposed models were incorporated to a nonlinear finite-element program COM3 (Maekawa 2003) by which all analyses in this paper were performed. The smeared, two-way fixed-crack approach based on the active crack concept was employed. In this scheme, nearly orthogonal cracks with the strongest nonlinearity are considered to be the active cracks. Along these cracks, the stress and strain of the ECC are computed.

### 2.6.1 Verification example 1: Pre-cracked ECC plates subjected to principal stress rotation

Eight ECC plates were tested under a four-point loading condition (Suryanto *et al*. 2010). The test parameters and details are listed in **Table 1**. Of the eight plates tested, the first two plates (Plates S1 and S2, 250×400×20mm), taken as control specimens, were loaded to a failure in a span of 340 mm, while the remaining six plates (Plate S3 to S8, 420×550×20mm), taken as the main plates, were pre-loaded in a span of 510 mm until the tensile strain at the bottom of the plates within the constant moment span reached either 40 or 70% of ultimate tensile strain $\varepsilon_{tu}$ [see Step A in **Fig. 6(b)**].

To eliminate the residual midspan displacement, the main plates were flipped upside down (Step B) and then re-loaded (Step C). Following this, the main plates were cut in a certain orientation and into the size of the control plates [see **Fig. 6(a)** and Step E in **Fig. 6(b)**]. The main purpose of the cutting process was to align the inclination of the principal stress direction along the longitudinal axis of the plate. Following the cutting process, the second loading stage began with the plates re-loaded until their failure. Since the pre-cracks were at a certain angle to the plate width (e.g.: 20, 45, and 70 deg), it was possible to induce tensile and shear stress stresses along the pre-cracks interface.

At the beginning of the second loading stage, it was observed that the response of the plates depended largely on the behavior of the pre-existing cracks. This observation will be discussed in the following paragraphs in a comparison with analysis predictions. It was also observed that, when the stress condition dictated, a new set of cracks formed at a different orientation, named here as secondary cracks. For clarity, **Fig. 6(c)** presents the crack pattern of Plates S4, S6, and S8 after

Table 1 Test parameters and results of pre-cracked ECC plates.

| Plate | Designation | Dimension | | | Initial Damage | | Test Results | |
|-------|-------------|-----------|-----------|-----------|-----------------|-----------------------|--------------|-----------|
| | | W | L | H | Angle[#] | Level | $P_u$ | $d_{Pu}$ |
| | | mm | mm | mm | deg | % of $\varepsilon_{tu}$ [&] | kN | mm |
| S1 | Control | 250 | 400 | 20 | – | – | 3.69 | 8.90 |
| S2 | Control | 250 | 400 | 20 | – | – | 3.76 | 9.12 |
| S3 | Main | 410 | 550 | 20 | 20 | 40 | 3.80 | 10.46 |
| S4 | Main | 410 | 550 | 20 | 20 | 70 | 3.60 | 10.24 |
| S5 | Main | 410 | 550 | 20 | 45 | 40 | 2.98 | 8.99 |
| S6 | Main | 410 | 550 | 20 | 45[$] | 70 | 3.25 | 11.38 |
| S7 | Main | 410 | 550 | 20 | 70 | 40 | 3.14 | 6.60 |
| S8 | Main | 410 | 550 | 20 | 70 | 70 | 2.57 | 10.48 |

[#]intended average pre-crack angle with respect to the width of the plate after the cut
[&]average tensile strain of bottom plate surface within the constant moment span of Plates S1 and S2 at the peak load
[$]intended value; the obtained value was approximately 40 degrees
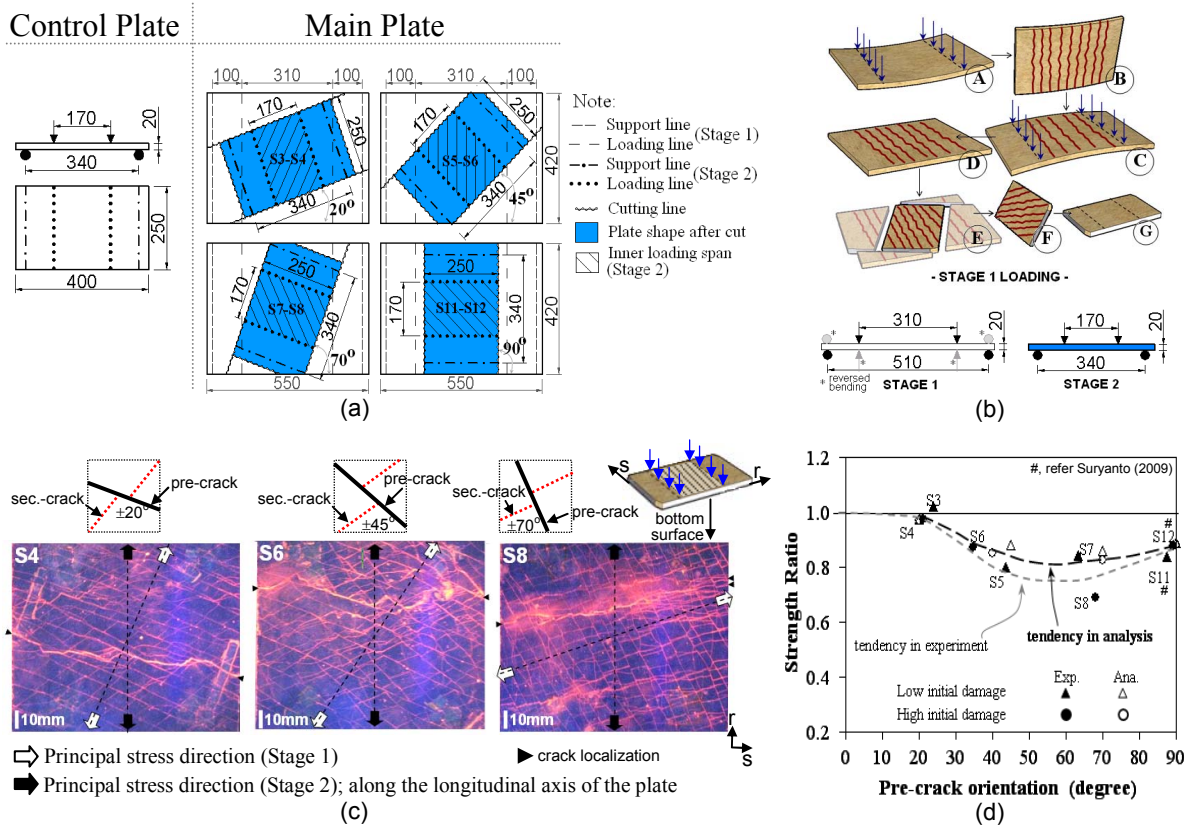


Fig. 6 Pre-cracked ECC plates experiment: (a) Layout of test plates; (b) Testing procedure, (c) Crack pattern of selected plates within the constant moment span at failure, and (d) Variation of load capacity with pre-crack orientation.

failure and within the constant moment span. It is evident from this figure that there are two sets of cracks: the pre-cracks and the resulting, secondary cracks. These two cracks are nearly orthogonal, forming a bi-directional crack pattern. This orthogonal crack pattern suggests that significant anisotropy is exhibited because of less stress transfer along the pre-cracks.

The response of the plates thereafter was dictated by the behavior of bi-directional cracks. The observed strengths for the eight plates are shown in **Fig. 6(d)**. The reduction in strength tends to increase with increasing pre-crack orientation and then begins to decrease when the orientation of the pre-crack approaches 90 degrees.

Numerical analysis was then conducted to examine the behaviors of the plates. **Figure 7(a)** shows the mesh used in the analysis. Each plate element was divided

into nine layers. The material properties used are as shown in **Fig. 7(b)**. The tensile properties were determined according to the predicted results which fit the response of the control plate [see **Fig. 7(c)**].

Similar to the testing procedure adopted, the analyses of the main plates were performed in two stages. *In the first stage*, the plates were loaded to a pre-determined degree of damage. The load was reversed and then unloaded until the midspan displacement of the plates was ultimately brought back to approximately zero. **Figure 7(c)**, for clarity, shows the response of main plates during the first loading stage. Afterwards, the cutting process was done by disengaging all the unnecessary elements, the non-shaded elements as shown in **Fig. 7(a)**. The boundary conditions were also updated so as the span and the inner loading span of the plates were 340 mm and 170 mm, respectively. As a result, the main plates were made to be essentially the same as the control plates. *In the second stage*, the loading was resumed

and continued until failure. Note that the response of the main plates during the second loading stage is determined by tensile and shear stress transfer along the bidirectional cracks. This provides a strict test of the proposed shear model and tension models.

To investigate the sensitivity of plate response to the shear transfer characteristics at the cracks, three types of analysis with three different shear transfer models were performed. In the first two runs, two different shear transfer resistance ($A$=0.50 and $A$=0.25) were considered and no shear softening was allowed. In the last run, the shear transfer resistance was assumed to be equal to 0.25 with a shear softening consideration.

**Figure 7(d)** and **(e)** compares the observed and predicted response of three plates with an initial damage of 70% $\varepsilon_{tu}$ and during the second loading stage in terms of applied load-versus-midspan displacement and applied load-versus-apparent strain across the cracks, respectively. Note that the apparent strain shown represents the
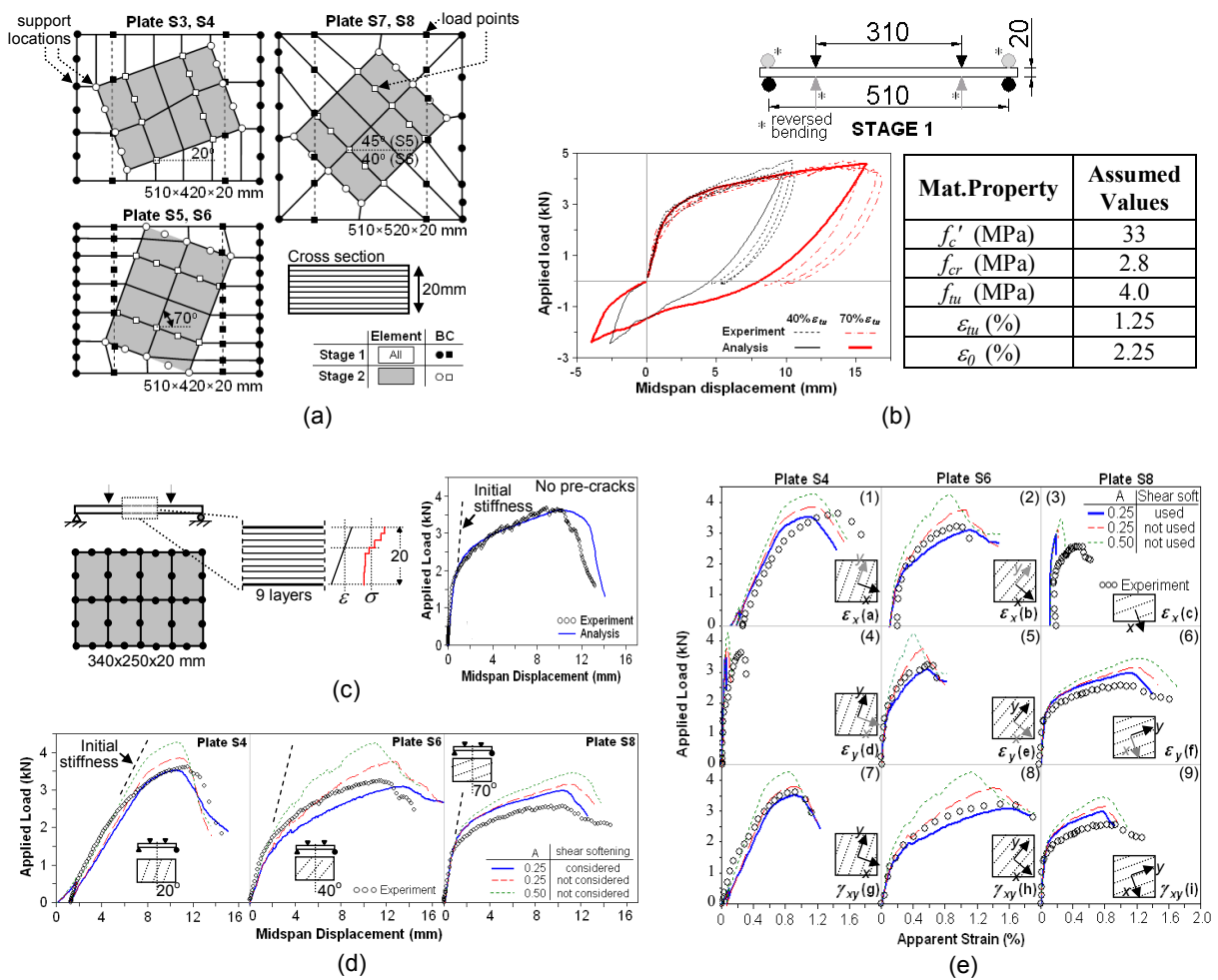


Fig. 7 Details of ECC plates analysis: (a) Mesh for analysis; (b) Comparison of analysis and experiments during stage 1 loading; (c) Comparison of load-mid displacement response of control plates; (d) Load-mid displacement response of pre-cracked plates; and (e) Applied load versus apparent strain at the bottom of the pre-cracked plates within the constant moment span.

average crack kinematics at the surface of the bottom plate within the constant moment span. All are presented in x-y coordinates (x-dir aligned with the direction of the pre-crack opening). It is evident from the figures that, at the early stage, both the observed and predicted responses of the plates are more sensitive to pre-existing damage (crack orientation and damage level) and less sensitive to the selection of shear transfer models. Specifically, the pre-existing damage results in a notable variation of initial stiffness in the load-displacement response as shown in **Fig. 7(d)** and in various patterns of crack-opening and -slip as shown in **Fig. 7(e)**. In one extreme, one can compare the response shown in **Fig. 7(d)** to that previously shown in **Fig. 7(c)**, which shows the response of Plate S1 with no initial damage. This finding highlights, once again, the need to accurately represent the effects of previous load history and damage, particularly when the applied load level is low. To this end, the predicted responses agree well with the observed response, demonstrating the viability of the proposed models in tracing damage.

At more advanced loading, the analysis results presented emphasize the importance of shear transfer. An overestimation of crack shear resistance (e.g.: $A$=0.50) results not only in significantly overestimated load capacity [see **Fig. 7(d)**], but also in significantly underestimated crack kinematics [see **Fig. 7(e)**]. This deficiency is particularly seen in Plate S6, where the crack-opening and -slip are significantly large [see **Fig. 7(e)–No. 2, 5, and 8**]. With a smaller coefficient reduction (e.g.: $A$=0.25), a better correlation is observed. Yet, the predicted load capacity and crack kinematics are still consistently higher and stiffer than the observed responses. The best prediction was obtained once shear softening is allowed. The analysis now was capable of capturing the observed strength degradation of the eight plates, as indicated by the mean of the observed-to-predicted strength of 0.99 and a coefficient variation of 8.2%. Another significant result is the close relationship obtained for the crack kinematics shown in **Fig. 7(e)**. This demonstrates that the proposed models replicate the kinematics of bi-directional multiple cracks well.

In summary, the verification study presented in this section shows that: (1) it is crucial to account for the previous load history if the behavior of an ECC element that has been sustaining damage is to be modeled; (2) the analysis results confirm the applicability of the proposed models to represent essential behaviors of ECC with multiple cracks in a strong anisotropy field, as indicated by the representation of the response of ECC plates sustaining various initial damage states; (3) an appropriate shear transfer model is necessary to predict the complete response of ECC when subjected to principal stress rotation.

### 2.6.2 Verification example 2: R/ECC plates subjected to principal stress rotation

A series of tests of six orthogonally-reinforced ECC

panels (890×890×70mm) were conducted by Xoxa (2003). Of the six panels tested, three panels (Panel PK4 to PK6) were reinforced with different reinforcement amounts in two orthogonal directions, thereby inducing an anisotropic condition during loading. Due to this difference, these three panels exhibit a more complex response. As the applied load increases, new cracks form at different inclinations while preexisting cracks open and exhibit pronounce slip. This then provides a difficult test to the proposed models, in particular, to the shear model. In this paper, the verification is focused on the responses of Panel PK5.

Panel PK5 was heavily reinforced in the longitudinal direction ($\rho_x$=4.56 %) and lightly reinforced in the transversal direction ($\rho_y$=1.027 %). Since the panel was fabricated with an evenly-distributed reinforcement and was uniformly stressed over its perimeter, the analysis was performed using only one square element as shown in **Fig. 8(a)**. A load-controlled scheme was employed. The material properties of the ECC and reinforcement were as reported by Xoxa (2003), except for the tensile property of ECC, which was determined to be close to that obtained from the panel test. This assumption was made since the tensile property of the ECC obtained from panel tests differed remarkably from that obtained from a coupon material test [for example, see **Fig. 8(b)**]. The difference was likely due to secondary effects such as fiber orientation and shrinkage.

To substantiate the assumption made regarding the tensile property, preliminary analysis was performed of which the results are shown in **Fig. 8(c)**. The analysis employed tensile property obtained from the reported material test [see T#1 in **Fig. 8(b)**] and three shear transfer models as used in the previous verification problem. One can observe from the figure that the accuracy of the predictions was poor. That is, the predicted response deviates significantly soon after first cracking, achieves a higher yield load value, and finally reaches peak load and deformation values grossly above the observed values. The poor prediction, as one may expect, is attributed to the overestimated tensile property.

To test this expectation, the panel was re-analyzed with a reduced tensile property (T#2, comparable to that observed from the panel test) in which the results are presented in **Fig. 8(d)**. Compared to the previous results shown in **Fig 8(c)**, it is very clear that a closer agreement to the observed response is obtained. Prior to the yielding of the transverse reinforcement, the predictions with the three shear models provide essentially the same response and agree well with the observed response. This is expected since the local crack slip during this loading phase is still limited. Soon after yielding, the difference among the three predictions is significant. This indicates that the yielding of transverse reinforcement causes a sudden lateral confinement loss to the cracks, leading to a significant crack opening and slip. Consequently, the post-yielding response of the panel is highly sensitive to the shear transfer model adopted.
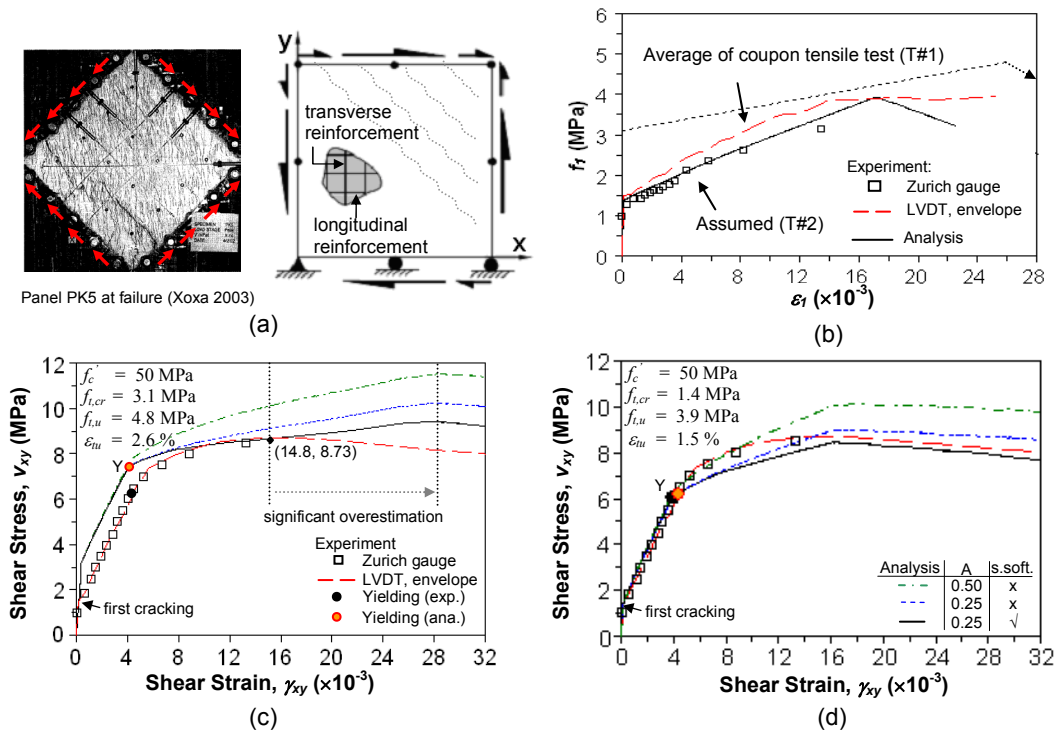
Fig. 8 Panel PK5: (a) Test panel and finite-element mesh; (b) Tensile stress-strain at the principal coordinate; (c) Shear stress-strain response employing tensile property from coupon test; and (d) Shear stress-strain response employing reduced tensile property.

Important aspects to these differences are summarized in the following paragraph.

The predicted response with $A=0.50$ shows a better agreement at a region directly after first yielding, but there was a significant overestimation of load capacity. In contrast, the prediction with $A=0.25$, with and without shear softening, overestimates shear deformation of the panel at a region shortly after yielding. However, it had a better load capacity prediction. The overestimated shear deformation with $A=0.25$ is likely attributed to simultaneous yielding of the transverse reinforcement rather than a gradual yielding as reported by Xoxa (2003). Hence, the prediction with $A=0.50$ at a region shortly after yielding appears in a better agreement. If the load capacity is of concern, accurate quantification of the actual shear transfer resistance is important and can be achieved with $A=0.25$, while the consideration of shear softening is *not* significantly important.

To give some indication of the importance of shear softening, consider the plots shown in **Fig. 9**. The plots correspond to the shear stress versus inclination of principal stress-strain and principal compressive stress versus principal compressive strain, respectively. One can observe from **Fig. 9(a)** that although the predictions employing the three shear models replicate the divergence angle of the principal stress and principal strain directions reasonably well, only that accounting

shear softening can reproduce the turning point of the inclination of the stress field. This occurring somewhat after yielding of the transverse reinforcement. This turning point indicates that the existing crack interfaces can no longer sustain the required shear stress, leading to an excessive slip along the cracks and eventually to a shear sliding failure. This behavior is well presented by the proposed shear model in which shear softening is allowed.

The significance of shear softening can also be seen from **Fig. 9(b)**, which shows the predicted and observed principal compressive stress-versus-compressive strain responses, plotted against cylinder test results. The agreement of the predicted responses employing the three shear models is good, all showing much softer responses than that obtained from a cylinder test. This soft response appears to be related to the rotation of the principal stress direction. Due to stress field rotation relative to the orientation of the preexisting cracks, local shear stresses are induced at cracks and contribute measurably to the compressive response at the principal direction. The soft response observed from the figure indicates the inadequacy of the cracks to transmit the required shear stresses.

It is evident from the figure that the predicted response for $A=0.25$ and the shear softening consideration provides the best correlation to the
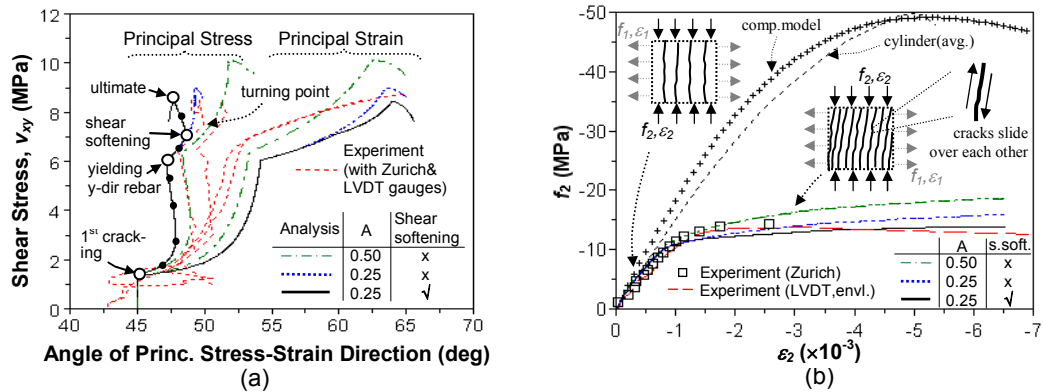
Fig. 9 Panel PK5: (a) Shear stress versus the inclination of principal stress and strain; and (b) Principal compressive stress versus principal compressive strain.

observed response. This is expected since the shear softening, as formulated, limits the ability of cracks to transmit shear stresses at large shear deformations. The best correlation observed validates the applicability of the shear softening equation previously shown in Eq. 9 to replicate essential shear stress transfer behaviors of ECC at large shear deformations.

Some important aspects from the verification example presented in this section are summarized as follows: 1) Tensile property in a R/ECC member may differ considerably from that obtained from uniaxial tensile test. The actual tensile property in a R/ECC member must be considered to provide accurate simulation of response; 2) It appears unnecessary to reduce the yield stress of reinforcement while it is embedded in ECC; 3) Accurate estimation of crack-shear stress resistance is important to obtain accurate shear strength prediction of the R/ECC element. As shown, it is the case with $A$=0.25 that provides an accurate shear strength prediction, indicating that the shear transfer resistance in cracked ECC is significantly less than that typically provided by aggregate interlock in concrete ($A$=1.0); and 4) The results shown validates the selection of $A$=0.25 and the consideration of shear softening for accurate representation of shear transfer across cracks in ECC. Not only must the model result in accurate shear strength prediction, it must also be able to represent internal stress carrying mechanism and the accompanying strain field.

To this end, the applicability of the numerical platform employing the proposed material models have been verified for element-level behavior under various damage states and in-plane stresses. Hereafter, its applicability will be tested for structure-level behavior.

## 3. Experiments on shear-critical RC and R/ECC beams

The experimental program conducted at the University of Michigan by Kanda (1998) was referred to. The experiment involved the testing of six beams with the following three parameters: material type (concrete and PVA-ECC), M/Vd ratio (1.0 and 0.5), and amount of transverse reinforcement (0% and 1%). The details of the six beams are illustrated in **Fig. 10** and are summarized in the following paragraph.

All the beams were 200 mm by 150 mm in cross-section. The main test region was the middle span; the span with maximum shear force $V$ as shown in **Fig. 10(a)**. To prevent flexural yielding and to promote shear failure inside the test region, all the beams were heavily reinforced in the longitudinal direction with twelve 13mm-diameter deformed bars [see **Fig. 10(b)**]. The property of the cement-based materials and the reinforcing bars is listed in **Table 2** and **Table 3**, respectively. Beams with transverse reinforcement (labeled -1) were expected to fail in shear-compression failure, whereas those without transverse reinforcement (labeled -0) were expected to fail in shear-tension. All beams were subjected to load-controlled cyclic loading by shifting the location of the boundary conditions horizontally as sketched in **Fig. 10(a)**. The overview of the test setup is given in **Fig. 10(c)**. For additional details regarding this experiment, one should refer to Kanda (1998).

### Approximate shear capacity

The approximate shear capacity of the test beams is determined from the AIJ shear design equation for RC. With different modifications, this equation has been used by various researchers for predicting the shear capacity of R/ECC beams (Kanda 1998; Nagai *et al* 2004; Shimizu *et al* 2004; Kanakubo *et al* 2007; among other). The modified equations vary, depending on the assumptions made on how the ECC contributes. Here, it is assumed that the tensile strength of ECC contributes to the truss mechanism after the formation of diagonal cracking, similar to that proposed by Nagai *et al* (2004). The modified equations are given by:
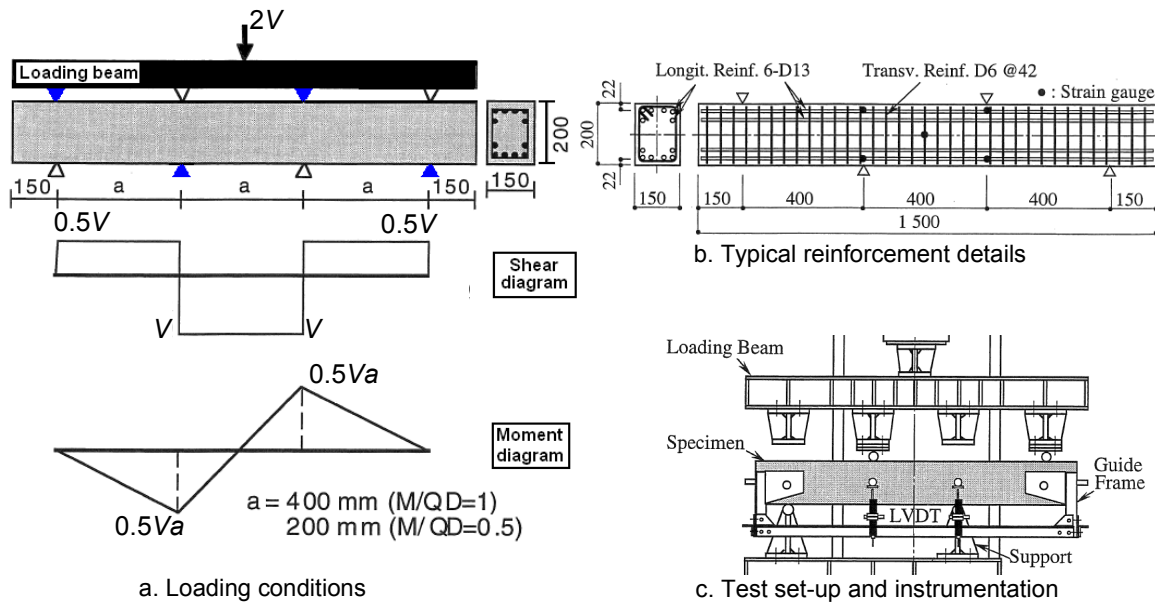
Fig. 10 Layout and test configuration of the shear beam (Kanda 1998).

Table 2 Material properties of cementitious material (Kanda 1998).

| Beam ID | $E$ (GPa) | Tension | | Compression | |
| --- | --- | --- | --- | --- | --- |
| | | $f_{tu}$ (MPa) | $\varepsilon_{tu}$ (%) | $fc'$ (MPa) | $\varepsilon_c'$ (%) |
| RC1-0 | 24.4 | 2.31 | – | 33.6 | 0.220 |
| RC1-1 | 23.9 | 2.55 | – | 30.5 | 0.192 |
| ECC1-0 | 12.8 | 2.61 | 1.40 | 45.7 | 0.484 |
| ECC1-1 | 13.0 | 3.57 | 3.34 | 41.2 | 0.451 |
| ECC05-0 | 13.4 | 3.38 | 1.21 | 41.6 | 0.384 |
| ECC05-1 | 12.8 | 3.38 | 1.21 | 40.1 | 0.406 |

Table 3 Material properties of reinforcing bars (Kanda 1998).

| Type | Bar size | $E_s$ (GPa) | $f_y$ (MPa) | $f_{tu}$ (MPa) |
| --- | --- | --- | --- | --- |
| Transverse | D6 | 194 | 364 | 406 |
| Longitudinal | D13 | 192 | 563 | 708 |

$$V = V_{truss} + V_{arch} = b\, j_t \left(\rho_w\, f_{y,w} + f_t\right)\cot\phi$$

$$+ \frac{1}{2}\tan\theta(1-\beta)b\, D\, \nu\, fc' \qquad (10)$$

$$\tan\theta = \sqrt{\left(L/D\right)^2 + 1} - \frac{L}{D} \qquad (11)$$

$$\beta = \frac{\left(1+\cot^2\phi\right)\rho_w f_{y,w} + f_t \cot^2\phi}{\nu f_c'} \qquad (12)$$

where $b$ and $D$ are the width and the depth of the member, respectively; $j_t$ is the distance between the top and bottom longitudinal reinforcement, $\rho_w$ is the web reinforcement ratio, $f_{y,w}$ is the yield stress of web reinforcement, $\theta$ is the angle of concrete strut in the arch mechanism, $\beta$ is the ratio of compressive stress of the concrete strut in the truss mechanism to the effective compressive strength of concrete, $\nu$ is a coefficient to account the effective compressive strength of the ECC and is assumed comparable to that of concrete, $f_c'$ is compressive strength of concrete, and "---" is a new term, accounting for the tensile strength of ECC.

### 3.1 Finite element analysis

Two-dimensional analyses were undertaken. Sixteen degree-of-freedom (16 dof) plate elements were used, but only its in-plane dof were used due to the two-dimensional problem concerned. Similar to that used in the verification problems presented earlier, the analysis employed a two-way fixed-crack approach incorporating the active crack concept.

Two typical finite-element meshes used to perform the calculation are illustrated in **Fig. 11**. The longitudinal bars were assumed to be smeared over the two outermost elements, while the transverse bars, if present, were smeared over all elements. As no information was given regarding the size of loading and support plates, it is assumed that the support and loading points are in contact with the beam at three nodal points in one element (see **Fig. 11**). The compressive and tensile strength of this element is assumed to be 50% higher to avoid premature computation termination due to the crushing of the ECC.

The analysis was performed in a manner as close as

possible to that in which the reversed cyclic load-controlled loading experiment was performed. At each load cycle, the boundary conditions were modified as sketched in **Fig. 11** (see Note #1 and #2 in the figure). Note that the support points were moved to the top of the beam, rather than shifted horizontally as in experiment. This shift is essentially similar and hence has no effect.

### 3.2 Comparison of experimental and analysis results of shear-critical beams
### 3.2.1 Benchmark analysis: RC beams with and without web reinforcement
To gain insight into the experimental condition and to

confirm the suitability of the FE modeling, Beams RC-10 and RC-11 were first analyzed. Since the cross-sectional size of the beams is small, it was felt that the influences of shrinkage, bleeding, and segregation of concrete were pronounced. As a result, non-uniform tensile concrete strength might exist across the cross-section of the beams. The heavy amounts of longitudinal reinforcement might also restrain the concrete, resulting in significant initial tensile stress and, accordingly, a lower tensile strength value. In this paper, a uniform tensile strength of concrete was assumed and the following two tensile strengths were specified to highlight the importance of suitable tensile properties: 1) tensile strength as reported ($f_t$, hereafter called T#1) and 2) re-



a. FE mesh of the beams with shear-span-to-depth-ratio 1.0



b. FE mesh of the beams with shear-span-to-depth-ratio 0.5

Note:
- ↔ ●—● Displacement monitoring point
- #1 BC in primary loading
- #2 BC in secondary loading
- B-C Main span
- ▮ Element containing smeared longitudinal reinforcement
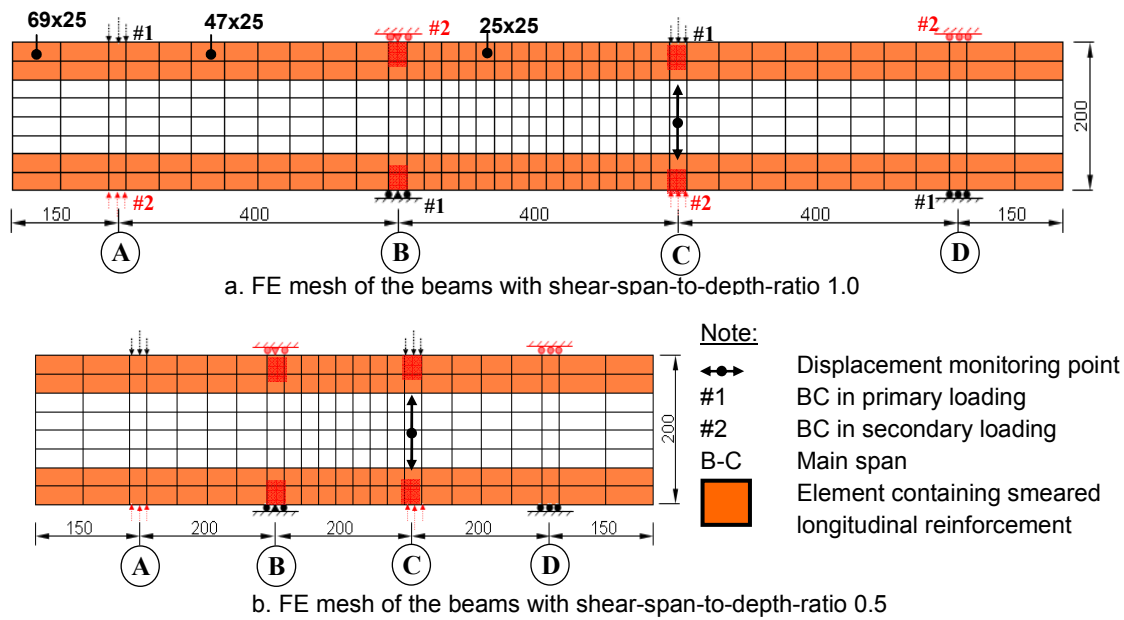
Fig. 11 Finite element mesh and boundary conditions.
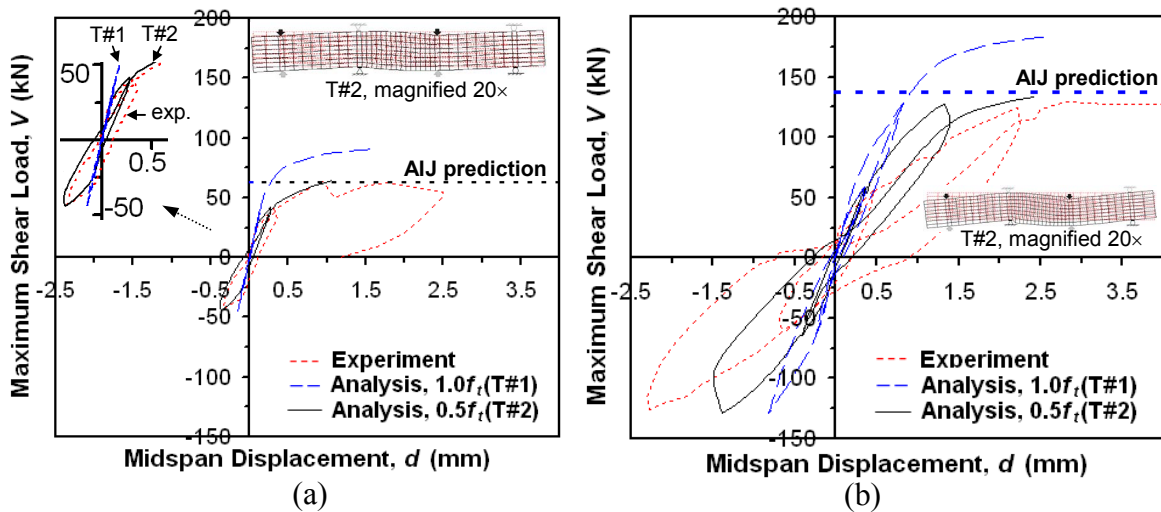


Fig. 12 Load-midspan Displacement Responses for RC beams with Shear-Span-to-Depth-Ratio 1.0: (a) RC1-0 (without stirrups); (b) RC1-1 (with stirrups).

duced tensile strength (50%$f_t$, T#2). The fracture energy of the concrete was assumed to be 0.070 N/mm, corresponding to a value computed for the corresponding compressive strength and with a maximum aggregate size of approximately 12-mm (Comité Euro-International Du Béton 1993).

### Analysis results

The load mid-span displacement response of RC1-0 and RC1-1 beams is shown in **Fig. 12**. The summary of the predicted and observed load capacity is listed in **Table 4**. The RC1-0 beam fails at the commencement of the third load cycle, whereas the RC1-1 beam fails at the fifth load cycle; both are similar to the experimental observation. By comparing the prediction results of T#1 and T#2, it is very clear that the beam response is strongly dictated by the ability of the concrete in resisting tensile stresses.

Compared to the observed load-displacement response, the predicted response employing the T#1 is much stiffer, the cracking load is about double and the beam capacity is about 50% higher. Employing the T#2, the test results now can be reproduced with a better correlation in the following two aspects: a closer capacity prediction, which is also comparable to the prediction by the AIJ shear design equation, and a better representation of the unloading-reloading response. This confirms the modeling of the beam, and hence it is ready for the analysis of the R/ ECC beams.

**Figure 13** shows a close agreement between the crack patterns predicted by the analysis and those observed experimentally. In Beam RC1-0, two major shear cracks began at the web zone along the main shear span

[see **Fig. 13(a)**] and then propagate progressively towards the loading and the support points. At approximately three-quarter of the central span, these two cracks are somewhat horizontal and then divert upward/downward to the region nearby the loading and support points. The cracking pattern observed in Beam RC1-1 is fairly similar and forms in a wider area.

### 3.2.2 Analysis on R/ECC shear beams
### Tensile and shear properties for beam analysis

Given the tensile property of ECC from material test, it is still unclear to what extent the data is applicable for structural analysis. One difficulty is the uncertainties related to the fiber orientation difference; the fiber orientation in a structural member is usually more random than in a coupon specimen, especially if the coupon specimen is thin and slim. Another difficulty is the way to account influencing factors as outlined in the previous section. At present, two tensile models are assumed to approximately represent the ECC in the test beams: T#1 and T#2. The T#1 is a model close to tensile stress-strain measured experimentally from coupon test, while the T#2 is T#1 reduced by 50% both at the peak stress and the strain corresponding to the peak stress. Note that it is more common to use a T#1-like property and properties of the other models (e.g.: compression, shear model) are calibrated to fit the macroscopic response. The comparison between the material test result of Beam ECC1-0 and the two tensile models is shown in **Fig. 14**. The tensile and compression properties used in the analysis are listed in **Table 5**, while the shear transfer property used were determined according to those identified from the verification examples presented in

Table 4 Comparison of RC shear beam capacity based on FE analysis, experiment, and modified AIJ shear design equation.

| Tensile Model | RC1-0 | | | | | RC1-1 | | | | |
|---|---|---|---|---|---|---|---|---|---|---|
| | $V_{ana}$ (kN) | $V_{exp}$ (kN) | $V_{AIJ}$ (kN) | $\dfrac{V_{ana}}{V_{exp}}$ | $\dfrac{V_{ana}}{V_{AIJ}}$ | $V_{ana}$ (kN) | $V_{exp}$ (kN) | $V_{AIJ}$ (kN) | $\dfrac{V_{ana}}{V_{exp}}$ | $\dfrac{V_{ana}}{V_{AIJ}}$ |
| 1 | 91.3 | 62.7 | 62.8 | 1.46 | 1.45 | 183.9 | 128 | 137.1 | 1.44 | 1.34 |
| 2 | 64.1 | | | 1.02 | 1.02 | 133.2 | | | 1.04 | 0.97 |
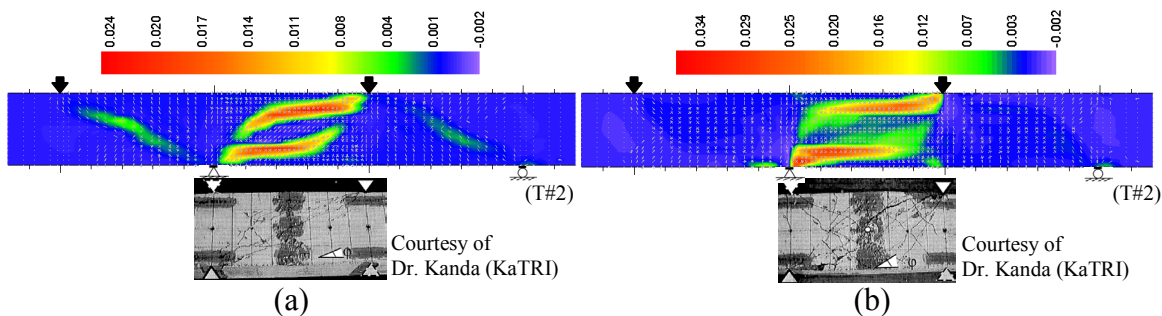


Fig. 13 Comparison of principal tensile strain-crack pattern for RC beams with shear-span-to-depth-ratio 1.0: (a) RC1-0 (without stirrups); (b) RC1-1 (with stirrups).

the earlier parts of this paper. The crack-shear transfer resistance ($A$) was set to 0.25 and shear softening was allowed.

### 3.2.3 Result of beam ECC1-0 analysis (without web reinforcement)

The comparison of the numerical and the experimental load-displacement response of Beam ECC1-0 are shown in **Fig. 15(a)**. The numerical results presented include the response predicted by the two tensile properties and the results reported by Kabele (2001, 2006). Presented in **Fig. 15(b)** is the predicted and observed crack pattern of the beam at failure; both agree and differ considerably from that of Beam RC1-0 previously shown in **Fig. 13(a)**.

The predicted response with T#1 shows a stiffer response and a higher shear carrying capacity. The beam is predicted to fail at a load of about 40 percent more than the observed capacity and about 15 percent less than the shear capacity predicted by the modified AIJ shear design equation (employing $f_t$) and at a corresponding displacement of 2.52 mm, about 20% less than the observed value. The predicted response if compared to those reported by Kabele (2001, 2006), which employed a comparable tensile property and a different shear model, also shows some discrepancies. The predicted strength presented here is slightly higher, while the predicted response is much stiffer. The discrepancy suggests that the shear model proposed herein tends to be stronger and much stiffer than those used by Kabele (2001, 2006).

When T#2 is employed in the analysis, a better agreement with the experimentally observed response is observed. Some notable improvements of the prediction
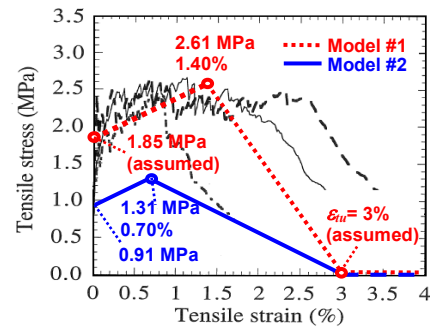


Fig. 14 Tensile models used for analysis Beam ECC1-0 plotted on the result of uniaxial tensile tests reported by Kanda (1998).

Table 5 Material properties used in the analysis of the ECC beams.

| Beam ID | Model | Tension | | | Compression | |
|---|---|---|---|---|---|---|
| | | $f_{cr}$ (MPa) | $f_{tu}$ (MPa) | $\varepsilon_{tu}$ (%) | $f_c'$ (MPa) | $\varepsilon_c'$ (%) |
| ECC1-0 | 1 | 1.80 | 2.61 | 1.40 | 45.7 | 0.484 |
| | 2 | 0.90 | 1.30 | 0.70 | | |
| ECC1-1 | 1 | 1.80 | 3.57 | 3.34 | 41.2 | 0.451 |
| | 2 | 0.90 | 1.79 | 1.67 | | |
| ECC05-0 | 1 | 2.70 | 3.38 | 1.21 | 41.6 | 0.384 |
| | 2 | 1.35 | 1.69 | 0.60 | | |
| ECC05-1 | 1 | 2.70 | 3.38 | 1.21 | 40.1 | 0.406 |
| | 2 | 1.35 | 1.69 | 0.60 | | |
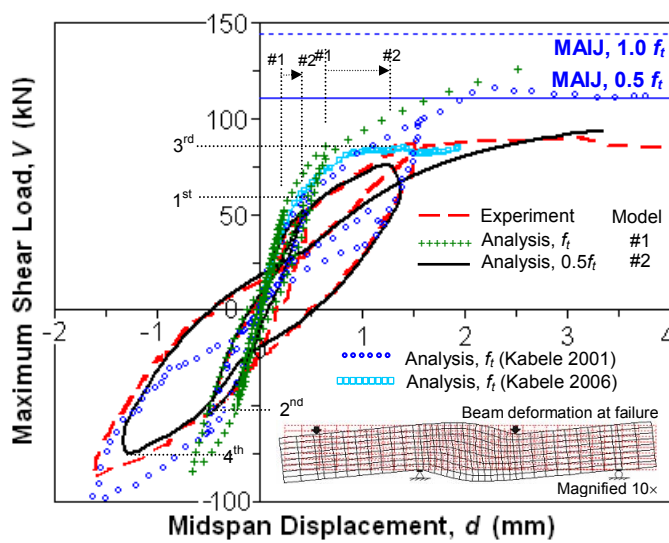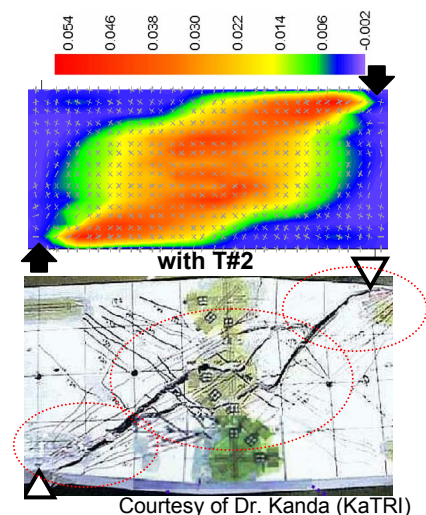


Fig. 15 Beam ECC1-0: (a) Load-displacement responses; (b) Crack pattern analytically predicted and experimentally obtained (Courtesy of Dr. Kanda, KaTRI).

are summarized as follows: 1) *Shear capacity*. The beam fails at 94.15 kN, which is about 5% higher than the observed value and about 15 percent less than the predicted value by the modified AIJ (employing $0.5f_t$); 2) *Maximum displacement*. The predicted displacement at the peak is 3.34 mm, which is about 5 percent more than the experimental value; 3) *Hysteretic loop*. The hysteretic loop is thick and in a close agreement with the observed loop. A more remarkable degree of pinching and stiffness degradation is observed; 4) *Residual displacement*. The residual displacements are significant and in the same order as the observed values.

To gain a sense regarding the involved mechanisms during cyclic loading, the plots of the principal tensile strain contour and the numerical crack pattern of the beam at the peak of each load cycle are given in **Fig. 16**. The color scale shown corresponds to the range of the maximum and minimum principal strain values at each load cycle. One can observe from the plots that the stress carrying mechanism during the loading changes remarkably, particularly after cracking (Plot A onwards). Compared to the crack pattern of Beam RC1-0 shown previously in **Fig. 13(a)**, it is very obvious that Beam ECC1-0 transmits stresses in a comparatively more complex manner. It is observed in Beam ECC that new cracks form at different locations and orientations while the preexisting crack propagates. Redistribution of stresses due to substantial damage at the web region is also evident (see Plot D), emphasizing that principal stress and strain directions during loading always rotate. At failure, a notable Z-crack pattern at the web region and shallow crack localization nearby the support points are observed; both are in a close agreement to the observed crack pattern [see **Fig. 15(b)**].

## 3.2.4 Result of beam ECC-11 analysis (with web reinforcement)

The comparison of the observed and predicted response of Beam ECC1-1 is shown in **Fig. 17** and is summarized in **Table 6**. Presented in **Fig. 17(b)** is the predicted and observed crack pattern of the beam at failure. The agreement is good; both show a comparable pattern and differ remarkably from that of Beam RC1-1 shown in **Fig. 13(b)**. Similar to the previous beam, the use of reduced tensile property T#2 again results in a better correlation. Here is the summary:

1) *Shear capacity*. The shear capacity of the beam is predicted at 207 kN and 194 kN, with T#1 and T#2, respectively. The values are approximately 10% and 5% higher than the observed value, and consistently less than the predicted values of the modified AIJ equation (about 15% and 5% less, employing $f_t$ and $0.5f_t$, respectively);

2) *Degradation of shear strength*. The degradation of shear strength occurring between load cycles 5 and 7 can be successfully simulated only with the T#2. The analysis predicts that the degradation occurs due to the yielding of the stirrups at the mid-height of the web region, preventing complete closure of the surrounding ECC. With T#1, the yielding of the stirrups is delayed and thereby no strength degradation is observed. This finding emphasizes the need to reduce the tensile property of the ECC;

3) *Displacement at the maximum and ultimate loads*. The displacement at the maximum shear load for the two tensile models has a predicted-to-observed ratio of about 0.5 and 0.8, respectively, while at ultimate of about 0.4 and 0.6, respectively. This significant underestimation is probably due to the flat response around the peak load, which is problematic for load-control compu-
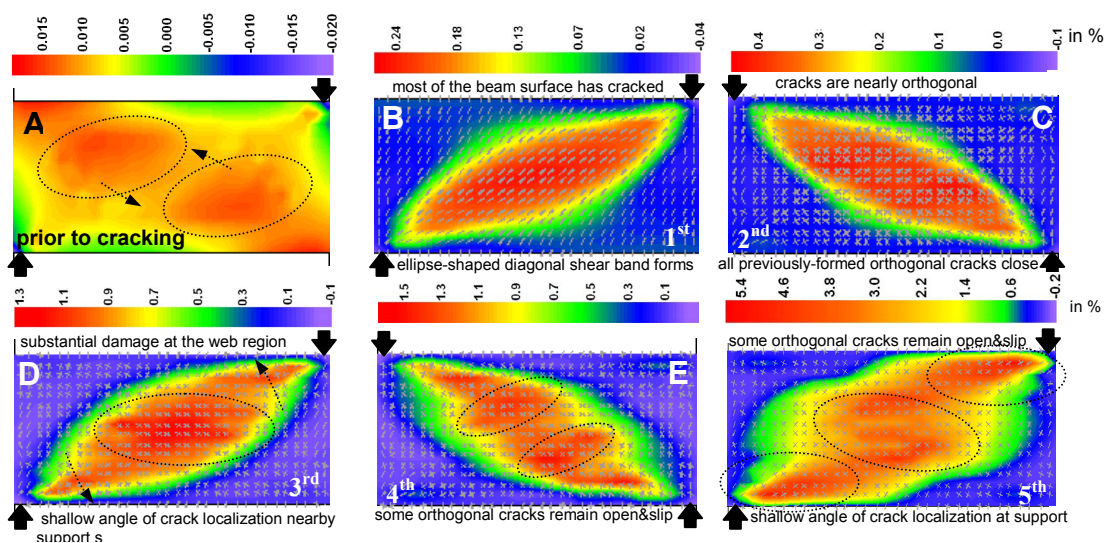


Fig. 16 Damage progress in beam ECC1-0 at the peak load of each load cycle.

Table 6 Comparison of beam capacity based on FE analysis, experiment, and modified AIJ shear design equation.

| Beam | Tensile Model | Max. Shear Load | | | | | Disp. at Max. Shear | | |
|---|---|---|---|---|---|---|---|---|---|
| | | $V_{ana}$ (kN) | $V_{exp}$ (kN) | $V_{M-AIJ}$ (kN) | $\dfrac{V_{ana}}{V_{exp}}$ | $\dfrac{V_{ana}}{V_{M-AIJ}}$ | $d_{Pu,\,ana}$ (mm) | $d_{Pu,\,exp}$ (mm) | $\dfrac{d_{Pu,ana}}{d_{Pu,\exp}}$ |
| ECC1-0 | 1 | 125.8 | 89.4 | 144.2 | 1.41 | 0.87 | 2.52 | 3.17 | 0.79 |
| | 2 | 94.2 | | 110.6 | 1.05 | 0.85 | 3.34 | | 1.05 |
| ECC1-1 | 1 | 207.3 | 186 | 244.6 | 1.11 | 0.85 | 2.0 | 5.8 | 0.34 |
| | 2 | 194.1 | | 198.6 | 1.04 | 0.97 | 3.3 | | 0.55 |
| ECC05-0 | 1 | 179.3 | 193 | 151.2 | 0.93 | 1.19 | 0.99 | 1.19 | 0.83 |
| | 2 | 165.2 | | 139.1 | 0.86 | 1.19 | 1.09 | | 0.92 |
| ECC05-1 | 1 | 227.2 | 262 | 213.7 | 0.87 | 1.06 | 1.33 | 1.32 | 1.00 |
| | 2 | 190.8 | | 186.6 | 0.73 | 1.02 | 1.62 | | 1.23 |
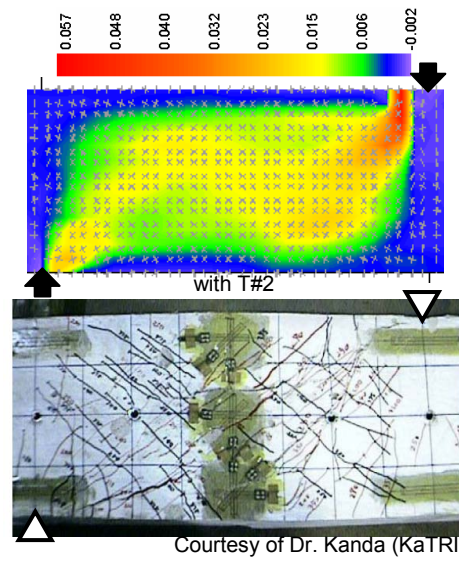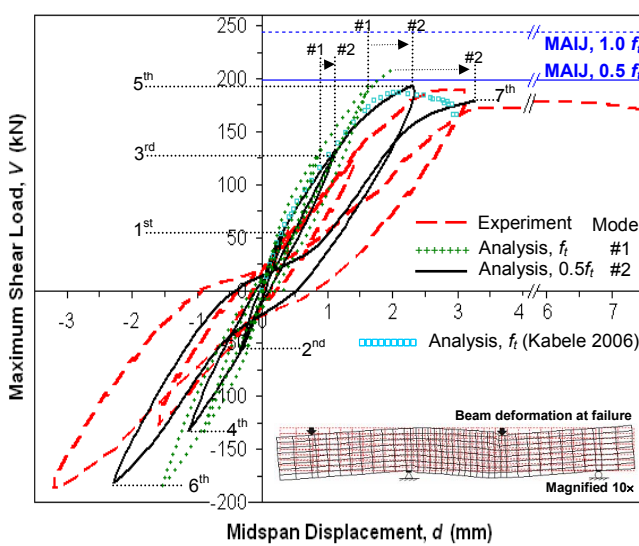


Fig. 17 Beam ECC1-1: (a) Load-displacement response; (b) Principal tensile strain versus crack pattern at failure (courtesy of Dr. Kanda, KaTRI).

tation;
4) *Hysteretic loop*. The predicted hysteretic loop of the beam is thin and narrow. From load cycle 5 onwards, only the T#2 can develop a notable amount of pinching and stiffness degradation, although the magnitudes are still smaller than the observed response;
5) *Residual displacement*. Notable residual displacement is observed only with the use of T#2, particularly once the stirrups have yielded.

**Figure 18** presents the principal tensile strain values of Beam ECC1-1 from loading cycle 3 onward. It is very evident from the figure that location of damage changes, particularly after the yielding of the web reinforcement (Plot C onwards). At the last loading cycle, the strain fields next to the support and the loading points are dominant, being slightly larger nearby the loading point. Although the failure may occur at both locations, the analysis shows that failure is ultimately

dictated by the crushing of the ECC next to the point load. The failure of the test beam tends to occur near to the support [see **Fig. 17(b)**].

### 3.2.5 Result of beam ECC05 series analysis (without and with web reinforcement)
This section briefly outlines the results of an analysis of short R/ECC beams with M/Vd ratio 0.5. **Figure 19** shows the observed behavior and the computed response for Beams ECC05-0 and ECC05-1. In this series, the analysis always underestimates the load capacity of the beams.

For Beam ECC05-0, the prediction result with both T#1 and T#2 predicts shear capacity consistently lower than the observed value, and higher than the modified AIJ shear design equation (see **Fig. 19**). The displacement at the peak load is approximately equal to that of the observed value. The predicted response by Kabele
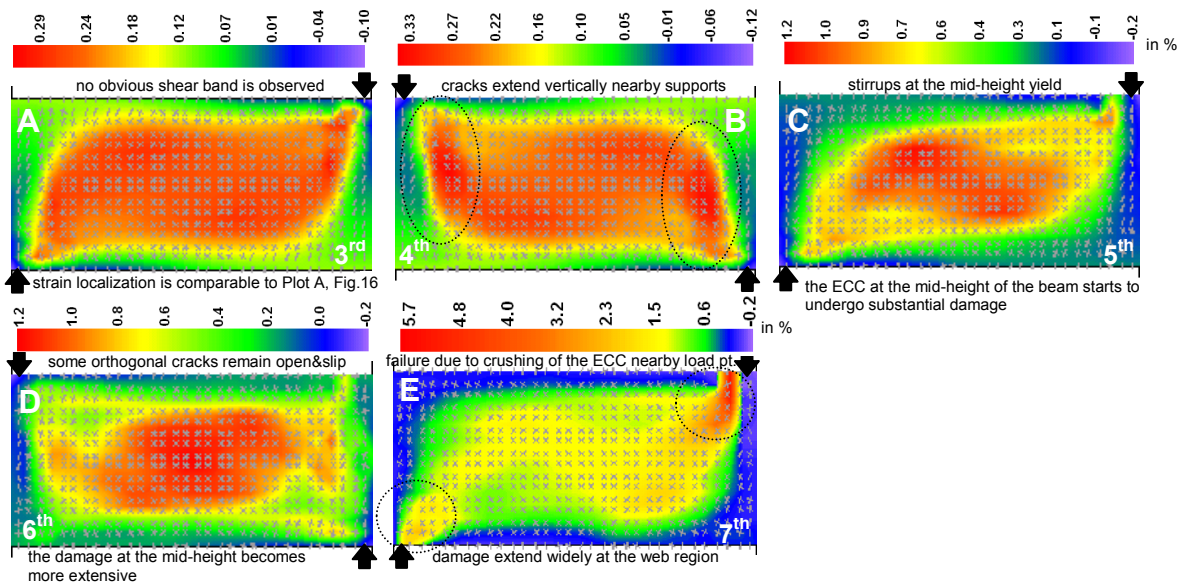
Fig. 18 Numerical crack evolution in Beam R/ECC1-1 from load cycle 3 onwards.
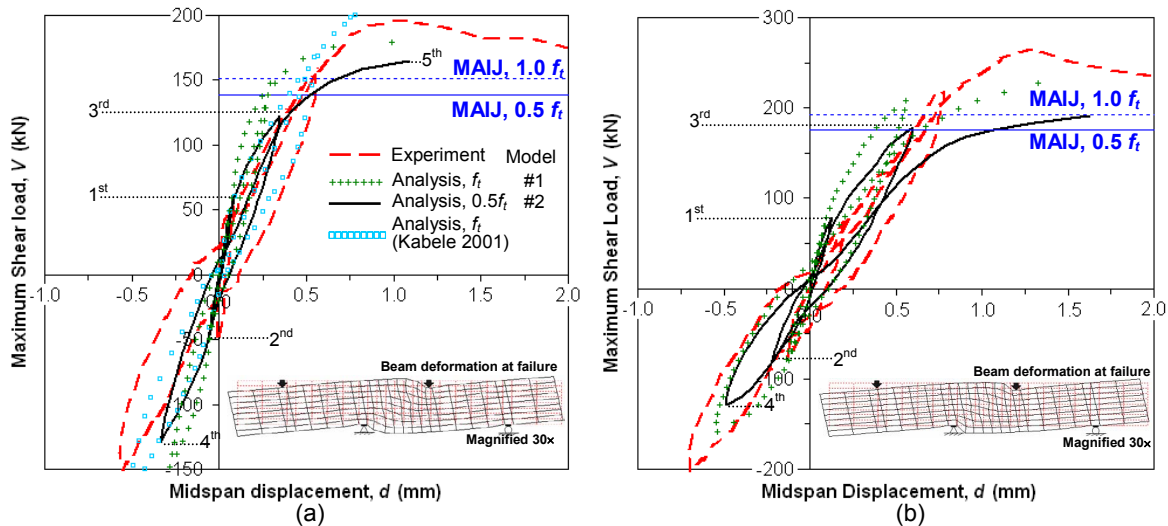


Fig. 19 Comparison of Load-Displacement Responses for: (a) Beams ECC05-0; and (b) ECC05-1.

(2001) is better and in a closer agreement to the observed response.

For Beam ECC05-1, the use of T#1 and T#2 also underestimates the beam capacity. The tendency is also similar to the previous beam. Unlike Beam ECC05-0, however, which the failure mode is expected to be due to extensive shear sliding at the diagonal compression strut [see **Fig. 20(a)**], the strain field of Beam ECC05-1 shown in **Fig. 20(b)** suggests that failure is dominated by the crushing of the ECC nearby the loading and support points. It appears that the predicted failures agree with the observed crack pattern from the test beams.

There might be two possibilities for the underestimated load capacity. The first possibility is the support

conditions. In the experiment, it is possible that the test rig restrained longitudinal deformation of the beam, allowing the direct compressive struts form from loading to support points, and thereby leading to an apparently higher shear capacity. To check this possibility, both beams were re-analyzed with pinned supports. The analysis results show that the shear capacity of the beams slightly increases from 165 kN and 191 kN to 170 kN and 200 kN, for Beams ECC05-0 and ECC05-1, respectively, indicating that the boundary conditions might *not* be the sole responsible factor. Another possibility is plate size. For a small M/Vd ratio, it is known that beam capacity is governed by the size of the diagonal compressive strut, which relates to the size of the
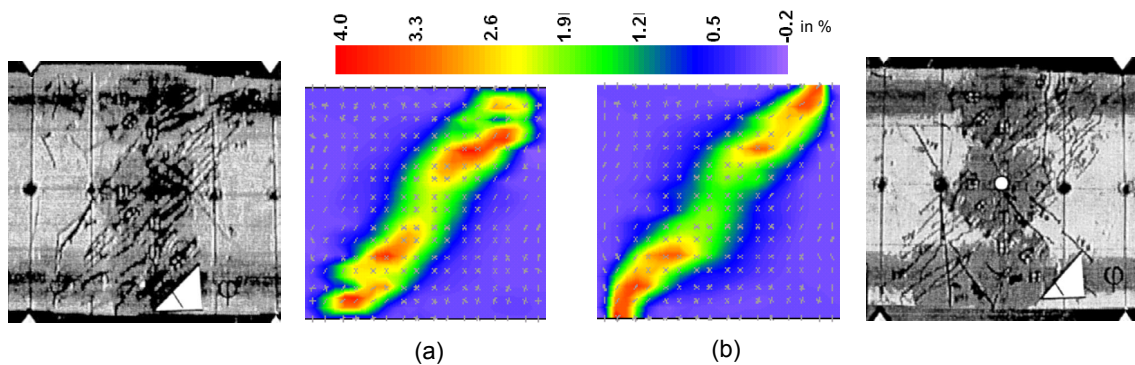
Fig. 20 Computed crack pattern of Beams ECC05-0 and ECC05-1 and the corresponding experimental crack pattern (Kanda 1998).

loading plates. The influence of plate size becomes significantly high as the shear span decreases. As larger plate size decreases the effective shear span, higher shear strength may result. Nevertheless, no additional analysis was performed since the actual size of the plate used was *not* reported, and hence it would be difficult to come up with a definite conclusion.

## 4. Conclusions

This paper presents the systematic development of nonlinear finite-element procedure in the context of a smeared, fixed crack approach for R/ECC members subjected to arbitrary loading. The smeared context employed allows a simple yet accurate representation of the fundamental behaviors of ECC without considering all details at every single crack in the ECC. Compression, tension, and shear transfer models of ECC in the context are proposed. Significant attention was paid to the modeling of shear transfer, which has received comparatively little attention in the past two decades, and the accuracy of the path-dependent formulations adopted in the models proposed. Two verification examples at an element level are presented to validate the proposed models, demonstrating that the models replicate various responses of cracked ECC in highly anisotropic stress and strain conditions. After confirming the applicability of the proposed models at an element level, the analysis procedure was used to simulate the behavior of a test series of shear-critical R/ECC beams subjected to reverse cyclic loading. Conclusions derived from all the simulations performed include the following:

1. Path-dependent, smeared models proposed are capable of providing reasonable characterization of damage progress and damage accumulation of ECC during reversed cyclic loading. In particular, the ability of the models to portray a higher degree of stiffness degradation, a larger value of residual displacement, and an increased degree of pinching in the load-displacement relationship as the degree of damage increases is verified.

2. The proposed models perform well in simulating the response of pre-damaged ECC plates subjected to stress field rotation. Load-displacement response and average strain across bi-directional cracks are equally well simulated, indicating that the proposed models are viable to account for the existing damage and to comply with non-proportional loading. Proper modeling of shear transfer plays a significant role for accurate simulation.

3. The result of an R/ECC panel test suggests that the tensile property of ECC in R/ECC and in a representative coupon, which is smaller in size and without embedded reinforcement, is considerably different. It is shown that the use of the tensile property as extracted from a panel test significantly increases the accuracy of the prediction, underscoring the need to estimate the actual ECC tensile property in  the R/ECC member. The detail response of the panel can be explained in a rational way. Further, it is demonstrated that shear softening consideration is necessary to reproduce the observed shear sliding failure.

4. Accurate analysis of an R/ECC beam relies on a proper representation of tensile and shear stress transfers of ECC at the cracks. When the identified shear transfer property was employed, it was found that the tensile property of ECC for analysis of the beams should *not* be simply obtained from a material test. Detail experimental investigations are in progress regarding this finding.

5. For R/ECC beams with M/Vd ratio of 1.0 and 150×200 mm cross-sectional size, with and without web reinforcement, the analysis shows that the influencing factors such as ECC shrinkage and material non-uniformity to tensile property of the ECC contributes measurably to the response of the beams. A reduced tensile strength and ductility of approximately 50% is appropriate for this experimental series to obtain reasonably accurate predictions of the loading capacity, hysteretic response, crack pattern, and failure mechanisms. In particular, the correlation of the observed-and-predicted hysteretic response and load capacity of the beams

improves significantly with a reduced tensile property.

6. The analysis shows that the governing failure mechanisms of the R/ECC beams are not only due to the breakdown of tensile stress transfer at cracks, but also of shear transfer mechanisms. Work is currently progressing on a possibility to improve interface shear transfer of a ductile cement-based material, likewise, ECC.

7. In a very short shear-critical R/ECC beam, having M/Vd ratio 0.5, it is shown that the modeling of the beams is more difficult. The proposed procedure somewhat underestimates the observed load capacity, although it predicts a correct failure mechanism. The cause of the underestimation appears to be the inaccuracy in modeling the loading plate.

## Acknowledgement

## References

An, X. (1996). "Failure analysis and evaluation of seismic performance for reinforced concrete in shear." Thesis (PhD). University of Tokyo.

Boshoff, W. P. and Van Zijl, G. (2007). "A computational model for strain-hardening fibre-reinforced cement-based composites." *Journal of the South African Institution of Civil Engineering*, 49(2), 24-31.

Comité Euro-International Du Béton (1993). "*CEB-FIP model code 1990: Design code*." Great Britain: Thomas Telford.

Fischer, G. and Li, V. C. (2002). "Influence of matrix ductility on tension-stiffening behavior of steel reinforced Engineered Cementitious Composites (ECC)." *ACI Structural Journal*, 99(1), 104-111.

Fukuyama, H., Sato, Y., Li, V. C., Matsuzaki, Y. and Mihashi, H. (2000). "Ductile Engineered Cementitious Composite elements for seismic structural applications." *In*: *12th World conference on earthquake engineering*, Auckland *30 January- 4 February 2000*. New Zealand: New Zeland Society for Earthquake Engineering, 1672/6/A.

Kabele, P. (1995). "*Analytical modeling and fracture analysis of Engineered Cementitious Composites*." Thesis (PhD). University of Tokyo.

Kabele, P., Takeuchi, S., Inaba, K. and Horii, H. (1999). "Performance of Engineered Cementitious Composites in repair and retrofit: analytical estimates." *In*: H. W. Reinhardt and A. E. Naaman, Eds. *Third international RILEM workshop High Performance Fiber Reinforced Cement Composites*, Mainz *16-19 May 1999*. France: RILEM Publications SARL, 617-627.

Kabele, P. (2001). "Assessment of structural performance of Engineered Cementitious Composites by computer simulation." Prague: Czech Technical University in Prague. CTU Report 4(5).

Kabele, P. (2003). "New developments in analytical modeling of mechanical behavior of ECC." *Journal of Advanced Concrete Technology*, 1(3), 253-264.

Kabele, P. (2004). "Linking scales in modeling of fracture in High Performance Fiber Reinforced Cementitious Composites." *In*: V. C. Li, Eds., *5th international conference on fracture mechanics of concrete and concrete structures*, Vail *12-16 April 2004*. FRAMCOS, 71-80.

Kabele, P. (2006). "Fracture behavior of shear-critical reinforced HPFRCC member." In: G. Fischer and V. C. Li, Ed., *International Workshop on High Performance Fiber Reinforced Cementitious Composites (HPFRCC) in Structural Applications*, *23-26 May 2005*. RILEM Publications, 383-392.

Kabele, P. (2007). "Multiscale framework for modeling of fracture in High Performance Fiber Reinforced Cementitious Composites." *Engineering Fracture Mechanics*, 74(1-2), 194-209.

Kanakubo, T., Shimizu, K., Kanda, T. and Nagai, S. (2007). "Evaluation of bending and shear capacities of HPFRCC members toward the structural application." *Hokkaido University COE workshop on High Performance Fiber Reinforced Composites for sustainable infrastructure system*, Sapporo *9 February 2007*, 35-44.

Kanda, T. (1998). "*Design of Engineered Cementitious Composites for ductile seismic resistant elements*." Thesis (PhD). University of Michigan.

Kanda, T., Watanabe, S. and Li, V. C. (1998). "Application of pseudo strain hardening cementitious composites to shear resistant structural elements." *In*: H. Mihashi and K. Rokugo, Ed. *3rd International Conference on Fracture Mechanics of Concrete Structures*, Gifu *12-16 October 1998*. Freiburg: AEDIFICATIO Publishers, 1477-1490.

Kato, B. (1979). "Mechanical properties of steel under load cycles idealizing seismic action." *CEB Bulletin D'Information*, 131, 7-27.

Kesner, K. E., Billington, S. L. and Douglas, K. S. (2003). "Cyclic response of highly ductile fiber-reinforced cement-based composites." *ACI Material Journal*, 100(5), 381-390.

Li, B., Maekawa, K. and Okamura, H. (1989). "Contact density model for stress transfer across cracks in concrete." *Journal of the faculty of engineering*, the University of Tokyo (B), 40(1), 9-52.

Li, V. C., Mishra, D. K., Naaman, A. E., Wight, J. K., LaFave, J. M., Wu, H. C. and Inada, Y. (1994). "On the shear behavior of Engineered Cementitious Composites." *Journal of Advanced Cement Based Materials*, 1(3), 142-149.

Shimizu, K., Kanakubo, T., Kanda, T. and Nagai, S. (2004). "Shear behavior of steel reinforced PVA-ECC

beams." 13th World Conference on Earthquake Engineering, Conference Proceedings DVD, Paper No. 704.

Maekawa, K., Pimanmas, A. and Okamura, H. (2003). "*Nonlinear mechanics of reinforced concrete.*" London: Spon Press.

Nagai, S., Kaneko, T., Kanda, T. and Maruta, M. (2004). "Structural capacity of reinforced PVA-ECC dampers." *6th International RILEM Symposium on Fibre Reinforced Concretes*, 1227-1236.

Suryanto, B., Nagai, K. and Maekawa, K. (2010). "Bi-directional multiple cracking tests of HPFRCC." *ACI Material Journal* (accepted for publication in 107(5)).

Suryanto, B. (2009). "Mechanics of high performance fiber reinforced cementitious composite subjected to principal stress rotation." Thesis (PhD). University of Tokyo.

Suwada, H. and Fukuyama, H. (2006a). "Experimental study on influencing factors on pseudo strain hardening behavior of High Performance Fiber Reinforced Cementitious Composite." *Journal of Structural and Construction Engineering AIJ*, 605, 1-8. (in Japanese)

Suwada, H. and Fukuyama, H. (2006b). "Nonlinear finite element analysis on shear failure of structural elements using High Performance Fiber Reinforced Cement Composite." *Journal of Advanced Concrete Technology*, 4(1), 45-57.

Xoxa, V. (2003). "Investigating the shear characteristics of high performance fiber reinforced concrete." Thesis (Master). University of Toronto.